Elsevier Editorial System(tm) for CARBON
Manuscript Draft

Manuscript Number: CARBON-D-18-03763R1

Title: Collapsed Carbon Nanotubes: From Nano to Mesoscale via Density Functional Theory-Based Tight-Binding Objective Molecular Modeling

Article Type: Research Paper

Corresponding Author: Professor Traian Dumitrica,

Corresponding Author's Institution:

First Author: Hao Xu

Order of Authors: Hao Xu; Grigorii Drozdov; Ben Hourahine; Jin Gyu Park; Rebekah Sweat; Thomas Frauenheim; Traian Dumitrica

Abstract: Due to the inherent spatial and temporal limitations of atomistic modeling and the lack of mesoscale models, mesoscopic simulation methods for guiding the development of super strong lightweight material systems comprising collapsed carbon nanotubes (CNTs) are missing. Here we establish a path for deriving ultra-coarse-grained mesoscopic distinct element method (mDEM) models directly from the quantum mechanical representation of a collapsed CNT. Atomistic calculations based on density functional theory-based tight-binding (DFTB) extended with Lennard-Jones interactions allow for the identification of the cross-section and elastic constants of an elastic beam idealization of a collapsed CNT. Application of the quantum treatment is possible due to the simplification in the number of atoms introduced by accounting for the helical and angular symmetries exhibited by twisted and bent CNTs. The modeling chain established here is suitable for deriving mesoscopic models for a variety of microscopic filaments with bending anisotropy.

Detailed Responses to Reviewers

Reviewer #1: In this short paper, the authors present a method to coarse-grain some mechanical properties (tension, torsion, and bending properties) of single- and double-walled collapsed CNTs using quantum-based simulations (DFTB+) at the fine scale and distinct element modeling at the larger scale, the passing parameter protocol being a classical one. The focus is given to the way the boundary conditions are applied at the atomistic scale and the concept of objective structures. This paper gives a relatively good description of the way the technique was implemented but should be significantly extended before a publication in Carbon could be considered.
Author reply: We thank the reviewer for clearly summarizing the paper and for recognizing that the presentation of the technical part is appropriate. This has given us confidence that we have got the message across in a concise way.

I would suggest the authors to:

-Extend the introduction and especially give a better view of the context to which their study is relevant.
Author reply: We thank the reviewer for the suggestion. In the recomposed manuscript, we have expanded the introduction to better communicate the experimental context, as well as the need for the development of mesoscopic models for collapsed CNTs. Specifically, the first paragraph of the introduction now makes it clear that we are targeting collapsed CNT assemblies resulted from the stretch-processing of raw sheets as these structures are interesting as material platforms for developing super strong lightweight composites. In the same paragraph, we have also discussed the unsuitability of the continuum simulation methods for the problem at hand, in order to better delineate the need for mesoscopic models. Finally, in the first paragraph of Section 4 (Summary and Conclusions) we have also mentioned the possible important implications of our model for designing ultra-strong CNT yarns made out of flexible collapsed CNTs.

-Validate their CG model against quantum or full atomistic simulations, moving then from a "verification" to a "validation"
Author reply: We thank the reviewer for the suggestion. The contact with the atomistic simulations can be achieved by comparing the strain energies of deformed CNTs as described by the two simulation methods. In the newly added Figure 6 we are showing twisted collapsed double-walled CNTs of two different lengths simulated at the CG level, followed by the atomistic DFTB level. The comparison discussed in the first paragraph of page 16 shows indeed excellent agreement for a case study that is experimentally relevant.

-Apply the CG model to a case study demonstrating the efficiency and accuracy of the proposed methodology.
Author reply: In the recomposed manuscript we made recourse to TEM images to identify relevant experimental cases, and to validate the developed model. The newly added Figure 6 contains TEM images of twisted collapsed CNTs which are double-walled CNTs (as it can be seen in Figure 6a) of ~6nm widths, and therefore can be modeled as (35,35)-(30,30) CNTs. As discussed in the newly added paragraph on page 16 (first paragraph on that page), the accuracy of the CG model in describing these experimentally relevant nanostructures is excellent. Additionally, the CG method is very efficient since these simulations took only a few minutes on a regular personal computer, as we stated in the same paragraph.

Moreover, could the authors comment on the following points:
-Large CNTs are generally composed of multiple walls not just one or two. To what extent modelling large SWCNTs and DWCNTs is then relevant?
Author reply: Indeed, a library of CG models for CNT composed of multiple walls will be eventually needed. As a typical first step in theoretical studies, one often starts the journey with simpler structures – single and double walled CNTs. We are currently at this first stage, where the main goal is to demonstrate the methodology for creating these models from an accurate quantum mechanical description of the interatomic interactions. The TEM images of the newly added Figure 6 comprise collapsed CNTs of ~6nm widths. (The number of walls can be identified from the high-resolution images of Fig. 6a). Thus, it is encouraging to see that the created model for the (35,35)-(30,30) CNT is already relevant for practical systems.

-Figures 3b,d, and f show CNTs submitted respectively to tension, torsion, and bending stresses. But all the pictures show similar (flat) geometries and are then confusing.
Author reply: Figures 3b, d, and f are displaying the ball-and-stick representations of the relaxed computational unit cells under the specified objective boundary conditions for tension, torsion, and bending. The geometrical deformations are indeed not obvious, since these deformations imply very little changes in the atomic positions. (As a side comment, it is comforting to realize that the macroscopic geometrical bending of an airplane wing implies very little stretching of the interatomic bonding!). However, these deformations become visible when formula (1) is applied to the relaxed atomic positions, as it was done in Figure 2. To make this clearer, we have added in the caption of Figure 3 that the geometrically deformed CNTs become visible when the unit cells displayed in b, d, and f are subjected to equation (1). Finally, we would like to clarify that our goal in showing these unit cells was to demonstrate that even under the largest considered deformations, the covalent bonds are not showing signs of fracture and that the collapsed shapes are actually undergoing changing very little with respect to the original cells under no stress conditions displayed in Figure 1a and b, this way supporting their lumping into a single distinct element "brick", Figure 1c.

-Why is there a need to implement special boundary conditions? Could the author draw a (quantitative) comparison with standard ways to impose tension, torsion, and bending stresses using MD like simulation techniques?
Author reply: Thank you for this question. The MD like approach relies on periodic boundary conditions (PBC), which are compatible to tensional deformation. The objective boundary conditions with helical angle zero are identical with the PBC ones. Therefore, the tensile deformation is applied in the standard manner. To impose a twist under PBC, one has to construct large simulation cells that have translational symmetry. The large number of atoms prevent the application of accurate quantum description of interatomic interactions, which are computationally expensive. In contrast, the number of atoms remains the same under objective boundary conditions, regardless the amount of twist. This makes affordable the application of the quantum treatment. Finally, the bending deformation is incompatible with PBC and this type of deformation is imposed with a cluster approach, which involves a large number of atoms and has deficiencies with imposing a pure bending. Instead, the objective boundaries allow for imposing pure bending by considering the small number of atoms located in the unit cells. In the recomposed manuscript, we made these differences clear in the added paragraph extending over pages 6 and 7.

-Parameters shown in Table 1 are not all defined in the text. It is also not clear how they have been obtained.
Author reply: Thank you for bringing up this point. As we now explained in the paragraph extended over pages 11 and 12, parameters C, K, D_s, and D_h are obtained by quadratic fits of the atomistic data for the strain energies of the unit cells restricted to the linear regime. By knowing these parameters, we can regain the strain energies stored in the unit cells under the different deformations. Parameters Y, G, w, and h are defined in the paragraph extending over pages 12 and 13. This paragraph also explains that Y, G, w, and h were obtained by equating the atomistic strain energies of the unit cells with those of an elastic continuum of same length. We hope that this part is much clearer with the addition of Figure 4, which ties the C, K, D_s, and D_h to the atomistic description, and Y, G, w, and h to the continuum one.

-Similarly, it is also not clear how the parameters shown in Table 3 have been obtained.
Author reply: As shown in the newly added Figure 4, all the parameters of Table 3 refers to the elastic parallel contact bonds between neighboring bricks. They can be redly obtained once the continuum intermediate idealization is in place (i.e, Y, G, w, and h are known.). Specifically, the spring constants have been obtained with the relations $k_n=Y/L$ and $k_s=G/L$ given on page 13 (toward the end). $A= hw$ is the cross-sectional area, as described on page 12 (end line). The expressions for $I_x=\frac{1}{12}hw^3$ $I_y=\frac{1}{12}wh^3$and $J_z=I_x+I_y$ are also given in the first paragraph of page 12.

Thank you again for the constructive input. A version of the manuscript with these marked points is also provided.

Reviewer #2: The authors describe a coarse-grained model to simulate collapsed carbon nanotubes, of interest in the context of carbon nanotube-based nano composites, which is constructed on the basis of

DFTB quantum mechanical calculations combined with an objective molecular modelling description to account for the bending and twisting of the specific nanotube examples that serve as a basis for determining the mechanical parameters that define the coarse grained model. Generally, the manuscript is clear and sufficiently well written, although it has a series of shortcomings that the authors should address before acceptance.

Author reply: We thank the reviewer for clearly summarizing the paper and for recognizing that the presentation and the idea of the paper are clear.

I find it unusual to have an introduction section that ends abruptly, without rounding up with a summary of the objectives of the work, nor setting out the structure of what follows. I think it would make the manuscript more readable if it adhered to convention on this point.

Author reply: We thank the reviewer for this suggestion. A paragraph describing the goal and structure of the paper was added at the end of Section 1 (paragraph extending over pages 4 and 5).

More technically, one wonders why the authors have chosen a mesoscale model that, judging from Figs. 1c and 4a looks like a piece of tape; presumably this is dictated by the form of the collapsed nanotubes, but wouldn't it be better to consider cylindrical collapsible shells that could account for both collapsed and uncollapsed nanotubes? The authors could better justify their choice of model.

Author reply: We thank the reviewer for this question. Indeed, a collapsible mesoscale model would be more powerful, but also significantly more expensive computationally. In the introduction section, second paragraph, we discuss one way of developing such model, essentially by coarse graining each wall of the CNT. (Such CG is currently done for modeling graphene – see Refs. 11 and 13) The level of CG in this approach would be low, and the intra-tube van der Waals interactions will be need in this approach. In the first paragraph of the introduction section we explain that we are targeting material systems containing already collapsed CNTs. Since modeling the cylindrical-to-collapse feature is not needed, and the collapsed CNT shape is robust under deformation (as our DFTB simulations show), we are pursuing directly an ultra-coarse graining, where each mesoscopic "brick" lumps hundreds of carbon atoms. Only with such an aggressive CG we will have a chance to uncover in the future the large-scale mechanics of these systems. We have modified the introductory section to better explain the above points. Additionally, in the conclusion section we have also explain the possible utility of our model for designing super strong carbon nanotube yarns comprising collapsed CNTs. A new supporting reference, Ref. 36, was added.

Finally, this reader is more familiar with atomistic simulations/models than with coarse-grained modelling, and I suspect that this will also be the case for the majority of this journal's readers. I think the authors could make a better job in describing in more detail the mesoscopic distinct element method used here, about which very little is said (certainly not enough to get a clear picture of it).

Author reply: We thank the reviewer for this suggestion. The mesoscopic distinct element method is in fact similar with MD with the difference that particles are evolved in time as rigid bodies, i.e. under the laws of classical mechanics $\mathbf{F}=m\ddot{\boldsymbol{X}}$ and $\mathbf{M}=I\dot{\boldsymbol{\omega}}$. This is explained in Section 3.2, where we have also added a whole new first paragraph on page 11 that offers a better picture of the mDEM method.

If the authors modify their manuscript according to these comments, I think the result will be a better manuscript that will not be out of place in Carbon.

Author reply: With the growing interest to the collective behavior of large diameter nanotubes for the benefit of applications, CG methods are becoming increasingly important; thus, it is not surprising that results obtained with the mesoscopic distinct element method have already appeared in Carbon, specifically in Ref. 33. Thank you for helping us improve the manuscript. A version of the manuscript with these marked points is also provided.

Abstract

Due to the inherent spatial and temporal limitations of atomistic modeling and the lack of mesoscale models, mesoscopic simulation methods for guiding the development of super strong lightweight material systems comprising collapsed carbon nanotubes (CNTs) are missing. Here we establish a path for deriving ultra-coarse-grained mesoscopic distinct element method (mDEM) models directly from the quantum mechanical representation of a collapsed CNT. Atomistic calculations based on density functional-based tight-binding (DFTB) extended with Lennard-Jones interactions allow for the identification of the cross-section and elastic constants of an elastic beam idealization of a collapsed CNT. Application of the quantum treatment is possible due to the simplification in the number of atoms introduced by accounting for the helical and angular symmetries exhibited by twisted and bent CNTs. The modeling chain established here is suitable for deriving mesoscopic models for a variety of microscopic filaments with bending anisotropy

1. Introduction

Advances in carbon nanotube (CNT) synthesis have brought a new class of materials, which include large volume CNT sheets suitable for developing macroscale applications [1]. The sheet exhibits a network structure comprising partially-aligned and entangled large-diameter CNTs. Currently, there are significant efforts to manipulate the CNT orientation by mechanical and electrochemical stretching of the CNT sheets [2]. During stretching, the initially cylindrical large-diameter CNTs undergo not only partial alignment and bundling, but also permanent radial collapse to a dog-bone-shaped cross-section [3, 4]. The resulted collapsed CNT assemblies represent a promising material platform for developing super strong lightweight composite materials with mechanical attributes approaching those of individual CNTs [1, 5, 6]. In this quest, the guidance power of computational materials modelling is critical for understanding how

materials properties are influenced by variations in structure at the mesoscale. Ideally one would like to simulate collapsed CNT assembles with all-atom simulation methods [7, 8], but this approach is computationally prohibitive. While large-scale mechanical behavior of materials is usually treated with continuum mechanics, simulation of the non-continuous response caused for example by the strain-induced relaxation of misaligned collapsed CNT bundles in a material with large void volume fraction, is not well adapted to the continuous description. Therefore, we are required to develop computationally efficient coarse-grained (CG) strategies, where the atomistic degrees of freedom are completely eliminated.

The dog-bone shape of the collapsed CNTs, Figure 1(a)-(b), is the outcome of the balance between the bending energy stored at the closed edges and the van der Waals (vdW) energy gained by bringing in close contact of the flattened CNT walls [9, 10]. In the quest of developing a mesoscale representation, one possibility is to pursue the CG of each one-atom thick graphene wall using the Martini force-field [11] or a Tersoff bond-order potential [12,13]. Such CG would capture the transformation from cylindrical to collapsed CNTs and therefore would be clearly needed if one would like to simulate the CNT stretching process [3,4]. However, this approach would be computationally ineffective for two reasons: first, the level of coarse-graining mapping will be low (a few carbon atoms to 1 CG element) and second, the developed effective potentials must be supplemented with long-ranged Lennard-Jones (L-J) interactions in order to describe the important vdW gluing of the flat faces. Since we are interested in resolving the representative mesoscale mechanics [14] of collapsed CNT assemblies, a more ambitious ultra-CG mapping (a few hundred carbon atoms to 1 CG element) capturing the carbon atoms in several unit cells is desirable. The development of such ultra-CG approach, which would capture implicitly into the effective potential the intra-tube vdW interactions, is supported by the observation that large

diameter collapsed CNTs (above ~4 nm in the case of single-wall CNTs) are stable [10] (do not go back to the cylindrical shape) and therefore can be regarded as individual entities. Furthermore, the strong covalent connection between the flat multilayer graphene central region enabled by the closed round edges, make the interlayer shear response significantly less important than in multi-layer graphene with free edges.

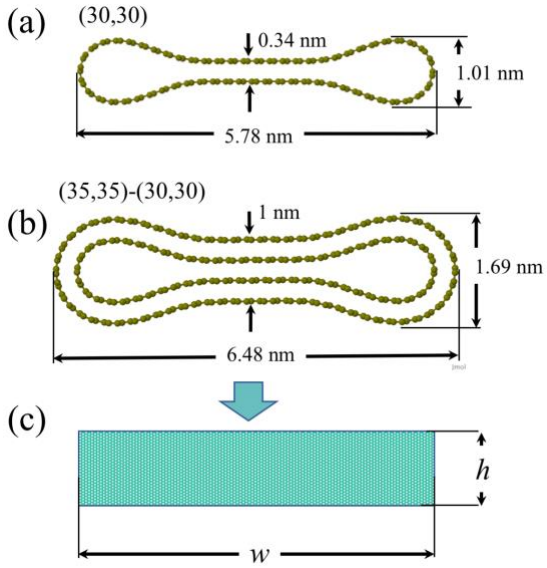

Figure 1. Cross section of the DFTB optimized (a) collapsed (30,30) single-wall CNT and (b) (35,35)-(30,30) double-walled CNTs. The number of carbon atoms N_o in the unit cells are 120 and 260, respectively. (c) Coarse grain "brick", representing carbon atoms in the unit cells.

While efficient ultra-CG methods for cylindrical CNTs have been already developed [14-17], such models for collapsed CNTs are currently missing. As a key step in addressing this issue, here we delineate a hierarchical multiscale chain in which objective molecular simulations [18] coupled with a quantum mechanical density functional-based tight-binding (DFTB) description of the interatomic interactions presented in Section 2, are used in Section 3.1 to uncover the nanomechanics of stretched, twisted, and bent collapsed single and double-walled collapsed CNTs. In Section 3.2, we transfer the obtained behavior to the meso-scale by developing a reduced-order

mesoscopic distinct element method (mDEM) model consisting of a chain of rigid "brick" distinct elements, Figure 1(c), connected by parallel bond contacts [17]. In Section 3.3, the mDEM model is verified and validated for describing the important twisting and bending deformation modes. Finally, Section 4 presents our summary and conclusions.

2. Model and Methods

Interatomic forces play a key role in establishing the shapes of the collapased CNTs resulted from the balance of bending strain stored one-atom thick hexagonal lattice and vdW adhesion. The selection of the interatomic potential is particularly subtle as the molecular mechanics of the commonly-employed bond-order potentials [12] describe bending strain differently [19]. As a result, the simulated nearly circular edges of the collapsed CNTs may present different shapes with different potentials [20]. Gao et al. [10] showed that force fields derived from density functional theory supplemented with Lennard-Jones (LJ) interactions can describe the shapes observed in experiment. Since force fields are less appropriate for describing the potential breaking of the carbon-carbon bonds at the reactive close edges, here we adopt instead the a tight-binding model with parameters derived from density functional theory [21] (DFTB) extended with L-J interactions (energy parameter $\varepsilon = 0.069$ kcal/mol and the distance parameter $\sigma = 3.80$ Å) similar with those used by Gao et al. [10]. While DFTB has been previously applied to collapsed CNTs [22-25], the focus was on CNT diameters less than the ones considered here. Moreover, we focus on simuations of collapsed CNTs under twisting, and bending deformations, Figure 2, which are enabled by the implementation of objective boundary conditions [18] into the code DFTB+ [26]. These boundary conditions are based on the concept of objective structures [27], and have been coupled [28] with DFTB in a manner that allows for the application of an arbitrary twist [25].

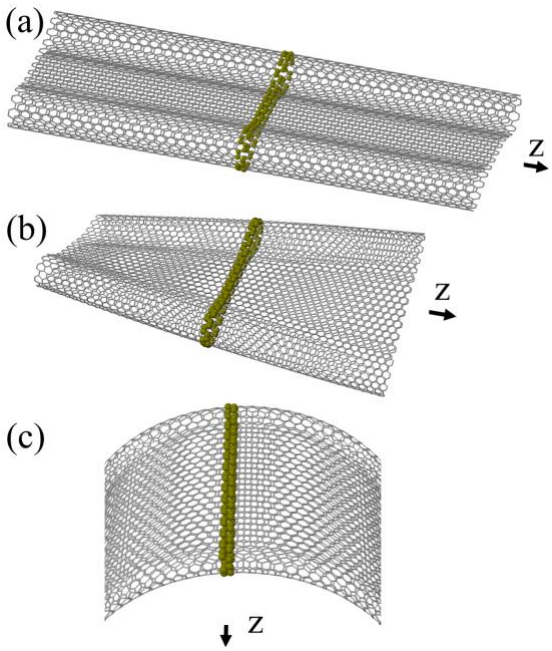

Figure 2. Relaxed configurations of (30,30) collapsed CNTs under (a) stretching, (b) torsion, and (c) bending. Helical boundary conditions are imposed along z axis. The simulation cells are shown as ball structures; the images obtained with eq. (1) are shown as wire frames.

It is worth to compare the traditional ways of imposing twisting and bending deformations, with the same deformations imposed by subjecting the N_o atoms of the unit simulation cell to objective boundary conditions. Uniformly twisted CNTs have a translationally repeating cell size corresponding to the size of the helical motif described by the closed edges. Such a large number of atoms (a multiple of N_o) makes unpractical alternative DFTB calculations adopting translational symmetry via standard periodic boundary conditions (PBC). Pure bending is a condition of stress where only a bending moment is applied to a CNT, without simultaneous application of axial forces. Since, a bent CNT is incompatible with PBC, this type of deformation is usually imposed in a cluster fixed-end approach, which involves a large number of atoms and where special care must be taken to relieve the axial strain in the CNT. Because under objective boundaries the only constraint imposed on the simulation cell is the bending angle, the N_o atoms are free to move away

or toward the rotation axis. The curvature of the CNT, is not imposed but is a result of the relaxation. Therefore, our method inherently tends to relieve the axial strain in the unit cells.

Our calculations considered collapsed (30,30) and (35,35)-(30,30) CNTs. The N_o atoms of coordinates $\mathbf{X}_{i,0}$ located in the simulation cell are imposed the objective boundary conditions

$$\mathbf{X}_{i,\zeta=}\zeta\mathbf{T}+\mathbf{R}^{\zeta}\mathbf{X}_{i,0}, \quad i=1,\ldots,N_o \qquad (1)$$

$$\mathbf{T}=\begin{bmatrix}0\\0\\T\end{bmatrix} \qquad \mathbf{R}=\begin{bmatrix}\cos\gamma & -\sin\gamma & 0\\ \sin\gamma & \cos\gamma & 0\\ 0 & 0 & 1\end{bmatrix}.$$

Here, $\mathbf{X}_{i,\zeta}$ are the coordinates of the ζ-th helical image of this atom, $\mathbf{T}$ and γ are the translation vector and angle comprising the helical operation. We describe next how these conditions allow to describe uniformly stretched, twisted, and bent collapsed CNTs: (i) With the boundary conditions expressed by equation (1), the standard translational case is regained by setting $\gamma=0^0$. An axial strain then can be applied by setting T around its relaxed state value T_0=2.47 Å. (ii) Figure 2b shows how an infinite collapsed (30,30) CNT, where $-\infty < \zeta < \infty$, under differential torsion (with $\gamma=1^0$) is described from a unit cell containing N_o=120 carbon atoms. To simulate this state, the twist angle γ acts as a constraint. The treatment of the long-ranged L-J interactions relies on a helical Ewald summation approach [29]. (iii) To simulate pure bending with eq. (1), T is set to zero and γ to $2\pi/N_a$, where N_a is an integer, and $\zeta = 0,\ldots,N_a-1$. This simulates a closed ring of constant radius R. The L-J interactions are calculated by direct real space summations. The collapsed shape introduces anisotropy. Bending along the closed edge direction is much harder than along the collapse direction, when the central one-atom thick layers undergo out-of-plane bending. In Figure 2c, we demonstrate the bending of the collapsed (30,30) CNT along the soft direction, with N_a=90. Simulating bending along the hard directions is done by re-orienting the unit cell such as the collapsed plane becomes perpendicular onto the z axis.

Conjugate-gradient relaxations carried out under the constrains (i)-(iii) were considered converged when the maximum atomic force was less than 10^{-4} Hartrees/Bohr. For the twist simulations, the electronic states were sampled over 20 uniformly distributed k helical points. For bending, all N_a angular points were considered to calculate the electronic energy. Our atomistic simulation results summarized in Figure 3 are discussed next.

3. Results

3.1 Objective DFTB Simulations of Collapsed CNTs

Previous atomistic calculations obtained that the failure elongation strains of defect-free cylindrical CNTs is about 14%-22%, depending on chirality [6], and that various defects can trigger fracture at smaller strains [30]. We find that the extended closed-edge "defects" are not promoting fracture and that the collapsed CNTs are not developing broken bonds up to the considered 12% strain. In fact, we find that the characteristic dimensions of the collapsed shape are changing very little, even at larger stretching, Figure 3(b). The computed strain energy, plotted in Figure 3(a), gives nearly quadratic overlapping curves for the stretching of collapsed (30,30) CNTs and (35,35)-(30,30) CNTs. The second derivative of the two overlapping curves of 64 eV is consistent with the stiffness of stretched graphene [19], indicating that overall the high curvature at the closed edges affects little the in-plane elasticity of the CNT walls.

The cross-sectional shape plays an important role in the torsional attributes of nanofilaments. Cylindrical CNTs are extremely stiff torsional springs [25], and for this reason this deformation is typically ignored in mesoscopic models [15]. By comparison, the collapsed CNTs are significantly less stiff under torsion since the hexagonal walls are storing less shear strain energy under a similar amount of differential twist [22, 25]. Thus, this deformation must be accounted for at the mesoscale especially in collapsed CNTs with fewer numbers of walls, Figure

3(c). The collapsed shape is again preserved under severe twisting, with the separation between flattened faces practically pinned at the 0.34 nm vdW equilibrium distance, and closed edges lacking any bond breakings, Figure 3(d).

Figure 3(e)-(f) and Figure S1 present our bending simulation results. The simulated behavior may be summarized as follows: initially, at low values of curvature, the CNT is in a state of pure bending with accumulation of in-plane elongation and compression strains on the opposite faces. The separation of the two strain energy curves with the number of layers in Figure 3(e) indicates that accumulation of strain is larger in the outer walls, which are more distant from the neutral bending plane. As curvature increases, the increased in-plane strain is accommodated by slightly decreasing the interlayer spacing in the central region, Figure 3(f), as well as the bulging of the edges away from the neutral surface with a width increase. Remarkably, this shape adjustment occurs without the breaking of any bonds located in the high curvature edges. By measuring the bending curvature at the different γ, we also noted that the $(\gamma\pi/180^0)/T_0$ approximation of the curvature is excellent. For example, for the configuration shown in Figure 3(f) the predicted bending radius is 3.55 nm while the one measured directly, by averaging the atomic positions, is 3.56 nm. We can conclude that like graphene, collapsed CNTs lack stretch-bending coupling up to fairly large curvatures.

The orders of magnitude differences between the extracted soft and hard bending constants D_s and D_h (Table 1) indicate that the collapsed CNTs exhibit a very strong bending preference along the soft direction. We previously studied the bending of 2-layer graphene, and obtained a bending stiffness of 163 eV [31]. Using this information, we can approximate the bending stiffness of the (30,30) CNTs containing 120 carbon atoms per cell as that of a bilayer with 60 atoms per layer, each taking up 2.71 $Å^2$ of area. We obtain 26,340 eV $Å^2$, which is close to our D_s fitted

value. The value approximated this way is below the computed one, indicating that the closed edges are reducing to some small extent the remarkable flexibility of collapsed (30,30) CNT.

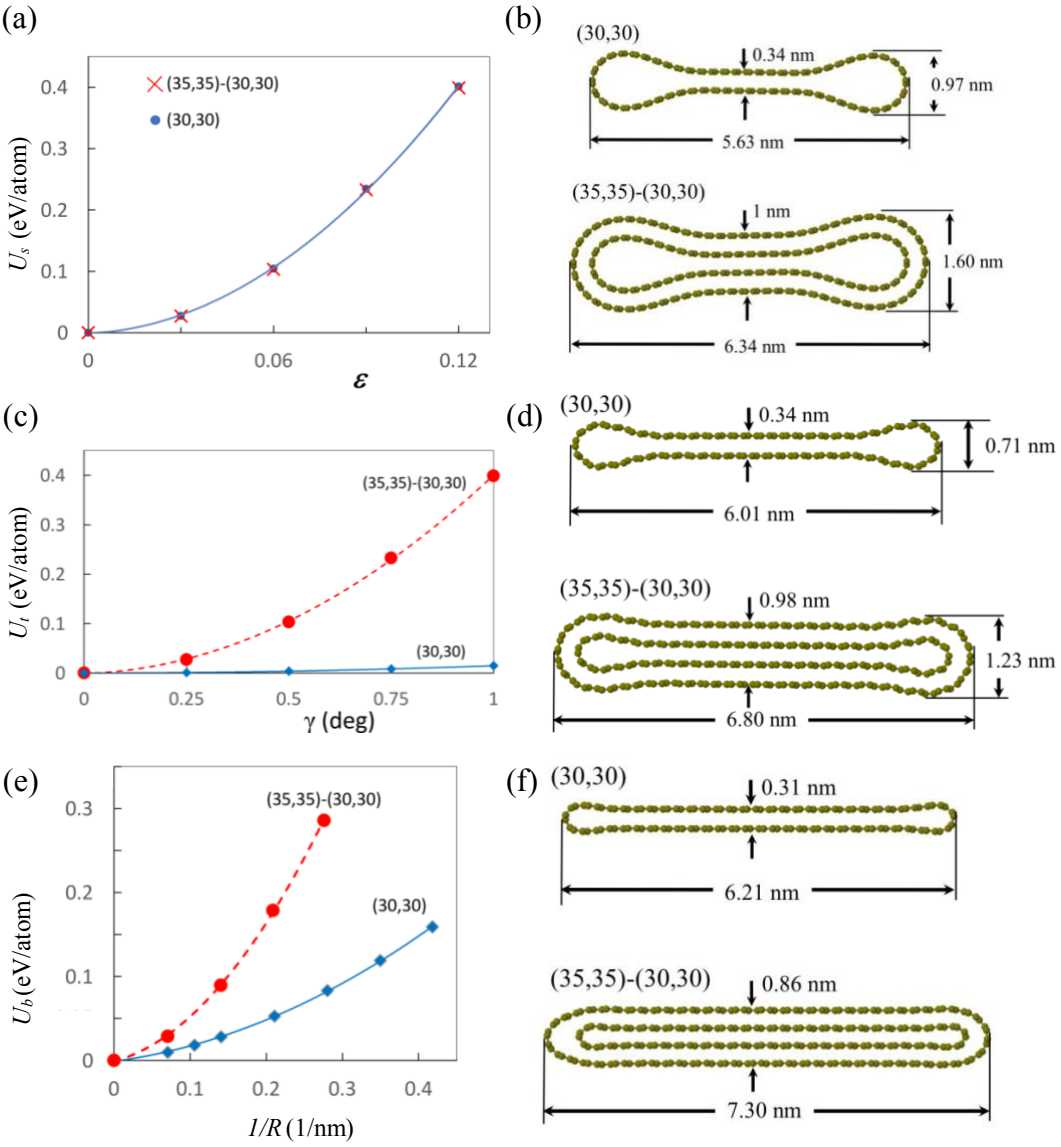

Figure 3. (a) Stretching energy vs. ε for (30,30) and (35,35)-(30,30) CNTs. Lines represent quadratic fits of the data points. (b) The relaxed shapes of the unit cells at ε=12%. (c) Torsional energy vs. γ. (d) The relaxed shapes of the twisted unit cells at γ=1^0. (e) Bending energy vs. $1/R$ (soft direction). (f) The relaxed shapes of the bent unit cells at γ=4^0 (N_a=90 and R=3.5 nm). The geometrically deformed CNTs become visible when the unit cells displayed in b, d, and f are subjected to equation (1).

3.2 Derivation of mDEM Models for Collapsed CNTs

DEM, the macroscopic method introduced 40 years ago by Cundall and Strack [22], is a numerical method that provides an explicit dynamical solution of the Newton's equation for a system of distinct bodies. While DEM is largely used today for simulating the mechanical properties of geological materials, we have adapted this method for cylindrical CNTs, where each CNT is represented by a chain of rigid cylindrical mesoscopic elements. The method is suitable for ultra-coarse graining since the mesoscopic elements are evolved deterministically in time as rigid bodies and therefore can track accurately for large grains. The mesoscopic elements are interacting with each other via contact models informed by atomistic scale simulations. Refs. [14] and [17] give detailed descriptions of how these microscopic interactions are incorporated into contact models for cylindrical CNTs, while Ref. [33] describes the application of mDEM to the mechanics of cylindrical CNT yarns.

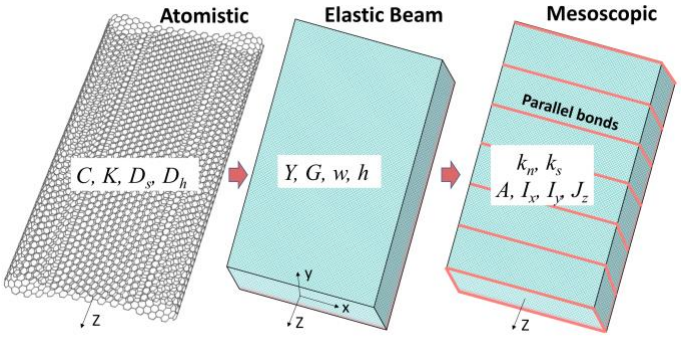

Figure 4. Representation of a collapsed CNT (left) as an isotropic elastic beam (center). Next, a collection of mesoscopic bricks connected by parallel bonds (right) are representing the inertial and elastic properties of the beam.

Figure 4 illustrates our strategy for developing the mDEM model for collapsed CNTs, which involves the intermediate step of setting an equivalent elastic continuum [17] based on the outcomes of the atomistic calculations. The stiffness constants C, K, D_s, and D_h of Table 1 are

obtained by direct fits of the DFTB data of Figure 3 and S1, restricted to the linear regime. With their help we can represent the stretching, twisting, and bending energies of the unit cells as $U_s = \frac{1}{2}C\varepsilon^2$, $U_t = \frac{1}{2}K\gamma^2$, and $U_b = \frac{1}{2}D_s(\frac{1}{R})^2$ and $U_b = \frac{1}{2}D_h(\frac{1}{R})^2$.

Table 1. Stiffness constants for (30,30) and (35,35)-(30,30) CNTs calculated with DFTB, and the material constants and cross-sectional parameters of the derived beam models.

CNT:	C (eV)	K (eV)	D_s (eV nm^2)	D_h (eV nm^2)	Y (TPa)	G (GPa)	w (nm)	h (nm)
(30,30)	7,697	13,520	300	25,630	1.15	37	6.32	0.68
(35,35)-(30,30)	15,401	82,824	2,404	60,696	1.27	102	6.57	1.31

We now focus on how to represent these deformations at the continuum level. While generally the elastic deformation of a nano-filament can be expressed in general with 10 elastic constants (to capture for instance cross-terms like bend-stretch coupling), the symmetries of the computed DFTB energy profile to clockwise and counter-clockwise twisting, and concave and convex bending of the collapsed CNT shape reduces significantly the number of independent constants. To this end, we propose to represent the DFTB computed energetics (encapsulated by C, K, D_s, and D_h) by an isotropic beam with rectangular cross-section which is uniform along the long axis. (A cylindrical cross-section was selected to represent cylindrical CNT [17].) The elastic energy of the beam is expressed as a summation of pure stretching, twisting, and bending strain energies along the soft and hard directions $U = U_s + U_t + U_b$.

The beam idealization is identified by equating the atomistic strain energy U of the unit cell deformed in a pure mode to that of a deformed beam portion of length T_0. In pure stretching, we have $U_s = \frac{1}{2}C\varepsilon^2 = \frac{1}{2}YAT_0\varepsilon^2$, where Y is the Young's modulus and $A = hw$ is the area of the beam

cross section. In pure twisting, $U_t = \frac{1}{2}K\gamma^2 = \frac{1}{2} G J_z \gamma^2 T_0$, where G is the beam torsional constant and J_z the polar moment of inertia. Finally, in pure bending along the soft and hard directions, we have $U_b = \frac{1}{2} D_s \left(\frac{1}{R}\right)^2 = \frac{1}{2} Y I_y T_0 \left(\frac{1}{R}\right)^2$ and $U_b = \frac{1}{2} D_h \left(\frac{1}{R}\right)^2 = \frac{1}{2} Y I_x T_0 \left(\frac{1}{R}\right)^2$, respectively, where $I_y = \frac{1}{12} w h^3$, $I_x = \frac{1}{12} h w^3$, and $J_z = I_x + I_y$. Solving these equations together, we arrived at the Y and G elastic constants, and the w and h parameters of the beam listed in the last columns of Table 1.

Having established the elastic beam idealization, we are now in the position to develop the mDEM model, by partitioning the beam into "bricks" of lengths L. Using the PFC3D [33] computational machinery of classical DEM, these elements will be evolved in time as rigid bodies (with 6 degrees of freedom per element). In mDEM, each "brick" element of dimensions h, w, and L, is evolved in time under the laws of classical mechanics $\mathbf{F} = m\ddot{\boldsymbol{X}}$ and $\mathbf{M} = I\dot{\boldsymbol{\omega}}$, where

$$\mathbf{I} = \begin{bmatrix} I_h & 0 & 0 \\ 0 & I_w & 0 \\ 0 & 0 & I_L \end{bmatrix} \qquad (2).$$

Here $\boldsymbol{X}$ labels the position of the center of mass and $\boldsymbol{\omega}$ the angular velocity of the element. The mass m and moments of inertia I_h, I_w, I_L components along the thickness, width, and length directions, respectively, of a "brick" with $L = 4T_0$, where $4N_o$ carbon atoms correspond to one distinct element, are summarized in Table 2. The elasticity of these elements is lumped into carefully designed parallel bond contacts distributed over the rectangular interfaces. The parallel contacts, which generate resisting forces $\mathbf{F}$ and moments $\mathbf{M}$, are essentially distributed linear springs with normal k_n and shear k_s stiffness (measured per unit area) representing the elastic response of a brick of length L, i.e. $k_n = Y/L$ and $k_s = G/L$ [17]. In Table 3, we are listing the parallel bond contact parameters for $L = 4T_0$.

Table 2. Parameters of the mesoscopic distinct element of "brick" shape with $L=4T_0$.

CNT:	L (nm)	m (amu)	I_h (amu nm^2)	I_w (amu nm^2)	I_L (amu nm^2)
(30,30)	0.99	5,765	19,660	693	19,411
(35,35)-(30,30)	0.99	12,491	45,951	2,806	46,717

Table 3. Derived parameters for the parallel bond contacts. The length of the element brick is $4T_0$.

CNT:	k_n (eV/nm^4)	k_s (eV/nm^4)	A (nm^2)	I_x (nm^4)	I_y (nm^4)	J_z (nm^4)
(30,30)	725	232	4.30	14.3	0.1	14.5
(35,35)-(30,30)	802	646	8.61	30.8	1.2	32.0

3.3 Verification and Validation of the mDEM Models

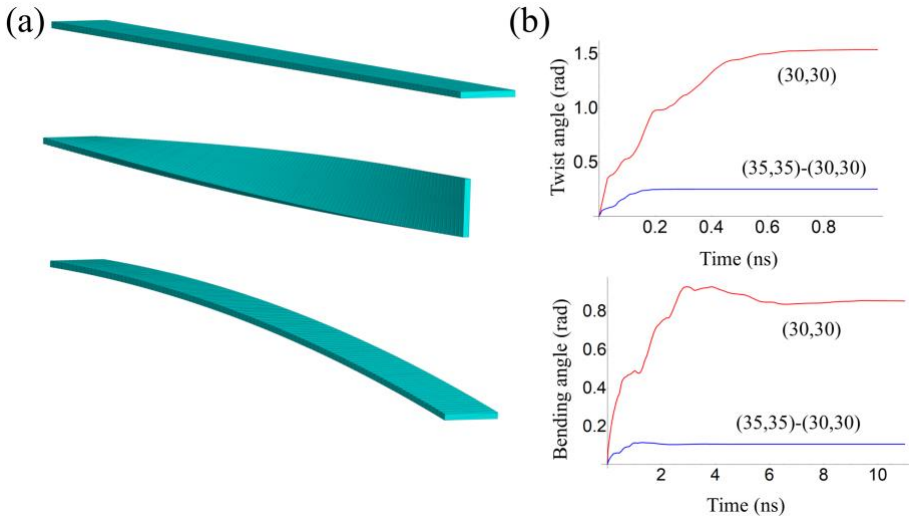

Figure 5. (a) mDEM simulations of a (30,30) collapsed CNT, stress free (top), and subjected to torsional (middle) and bending (bottom) moments. (b) Evolution of the total angular displacement of the element at the tip, when the collapsed (30,30) and (35,35)-(30,30) CNTs are subjected to a 50 eV twist (top) and 1 eV bending (bottom) moments.

In Figure 5 we provide a verification of the mDEM models for describing the important twisting and bending deformation modes. The (30,30) and (35,35)-(30,30) collapsed CNTs were

modeled by joining together 100 mesoscopic elements with the mass and moment of inertias given in Table 2, and the parametrization of the parallel bonds given in Table 3. In the initially straight CNT, the total contact forces and moments are set to zero. The velocities of all six degrees of freedom are fixed to zero for the first element, while an external twisting moment and an external bending moment along the soft direction, are applied separately to the last element, Figure 4(a). The deformation of the chain of bonded elements under the considered external loads results in relative twist ($\Delta\theta_w$) and bending ($\Delta\theta_h$) angles between elements. Restoring shear M_s and bending M_b contact moments are developed according to the incremental laws $\Delta M_s = -k_s J_z \Delta\theta_w$ and $\Delta M_b = -k_n I_y \Delta\theta_h$. The models are evolved in time with a 30 fs time step based on a velocity Verlet algorithm for translations and a fourth-order Runge–Kutta algorithm for rotations until equilibrium is reached. Figure 4(b) presents the accumulated angular displacements at the tip. The resulted values of 1.5381 rad (0.2510 rad) for twisting angle and 0.0851 rad (0.0106 rad) for bending of the single (double-) walled CNTs, agree within 4 significant digits to the closed form solutions $100LM_s/GJ_z$ and $100LM_b/YI_y$.

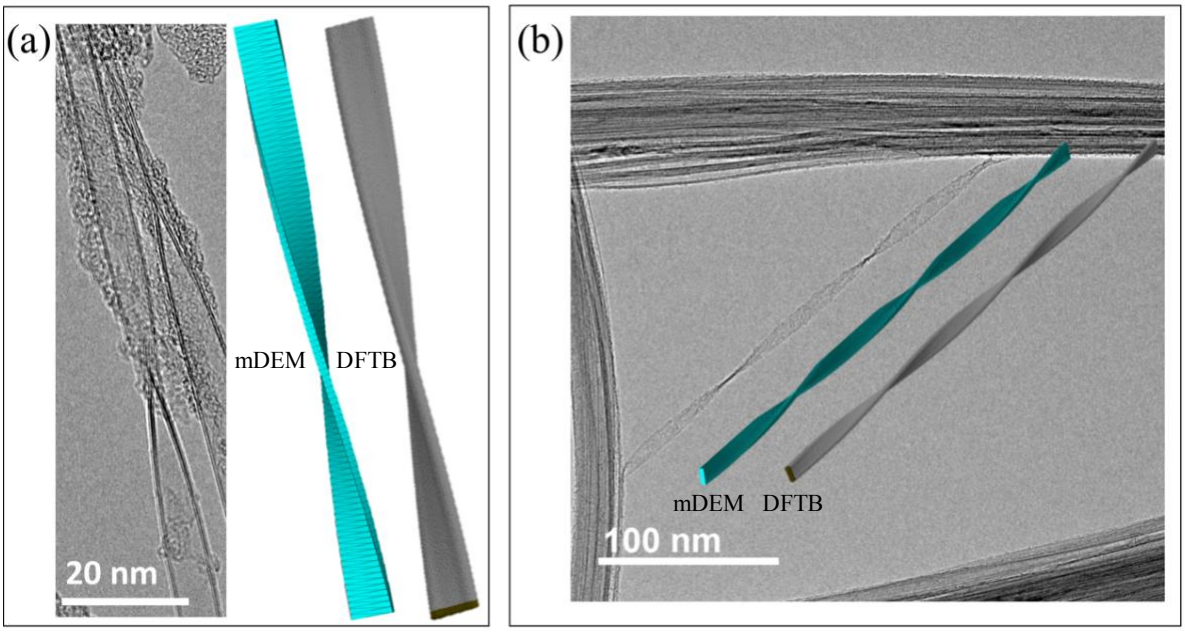

Figure 6. TEM images of pre-stretched CNT material, showing (a) a ~100 nm twisted collapsed double-walled CNT and (b) a ~300 nm twisted collapsed double-walled CNT located near the crossing of two CNT bundles. The mDEM and DFTB simulated (35,35)-(30,30) CNTs are shown near the experimental images.

As demonstrated in the TEM images of Figure 6, twisted collapsed CNTs are often encountered in the Nanocomp CNT sheets processed by stretching [2]. The experimental images are showing twisted double-walled CNTs collapsed to a ~6 nm width. The relative twist angles across the lengths of ~100 nm and ~300 nm are π and 3π, respectively. Interestingly, the stability of the twisted CNT of Fig. 6(b) can be likely explained by the competition between torsional energy stored in the individual CNT and the van der Waals adhesion energy of its ends with the crossed bundles. With mDEM, we modeled these filaments as twisted collapsed (35,35)-(30,30) CNTs comprising 100, Fig. 6(a), and 300, Fig. 6(b) mesoscopic distinct elements. To match the experimentally observed twist, the magnitude of the moment applied to the end element was determined with as $\pi G J_z/100L$. The cantilever set-up simulations took only a few minutes on a personal computer. The final twist angles are indeed π and 3π, and strain energy is 1021.8 eV and 3065.4 eV, Figure S2. These energies are in excellent agreement with the DFTB strain energy of 2.554 eV computed of the (35,35)-(30,3) collapsed CNT unit cell under $\gamma=0.45^0$ differential twist.

4. Summary and Conclusion

Objective simulations provided a detailed nanomechanical characterization of collapsed (30,30) and (35,35)-(30,30) CNTs, and obtained that the collapsed shapes are robust to severe stretching, twisting, and bending deformations. On this basis, we developed ultra CG mDEM models, able to quantitatively reproduce the nanomechanical response derived from the covalent and vdW intra-tube interactions. Owing to recent advances in characterization and capturing the

dynamical friction [35] and inter-tube shear between CNTs represented at the ultra CG level [16, 17], the derived mDEM models will be useful for simulating the mechanics of material systems comprising collapsed CNTs obtained by sheet stretching [2]. Recent modeling [36] revealed that bending rigidity of CNTs impacts, among other factors, the strength of CNT yarn, with the more flexible CNTs making stronger yarns. As our DFTB calculations showed, collapsed CNTs present extraordinary flexibility, comparable to that of few-layer graphene. Therefore, the mesoscale models developed here can prove useful for developing ultra-strong yarns by a computationally-guided design.

The multiscale chain established here and summarized in Figure 4 has implications beyond CNTs. With the helical Ewald rule approach [29], objective simulations are now possible with the self-consistent charge (SCC)-DFTB level of chemistry [37], which allows one to tackle the nanomechanics of a large variety of nano- and bio-structures, like DNA and actin. Thus, the multiscale modeling chain proposed here can be used to derive CG models from a quantum mechanical basis for a variety of complex microscopic filaments [38].

Acknowledgements

This work was supported by NSF Grant No. CMMI-1332228, NASA's Space Technology Research Grant NNX16AE03G, and by the Institute for Ultra-Strong Composites by Computational Design, Grant NNX17AJ32G. Resources supporting this work were provided by the Minnesota Supercomputing Institute and by NASA High End Computing Program through the NASA Advanced Supercomputing Division at Ames Research Center.

References

[1] E.J. Siochi, J.S. Harrison, Structural Nanocomposites for Aerospace Applications, MRS Bulletin 40 (2015) 829–835.

[2] S. Li, J.G. Park, Z. Liang, T. Siegrist, T. Liu, M. Zhang, Q. Cheng, B. Wang, C. Zhang, In Situ Characterization of Structural Changes and the Fraction of Aligned Carbon Nanotube Networks Produced by Stretching, Carbon 50 (2012) 3859–3867.

[3] R.D. Downes, A. Hao, J.G. Park, Y.-F. Su, R. Liang, B.D. Jensen, E.J. Siochi, K.E. Wise, Geometrically Constrained Self-Assembly and Crystal Packing of Flattened and Aligned Carbon Nanotubes, Carbon 93 (2015) 953–966.

[4] N.G. Chopra, L.X. Benedict, V.H. Crespi, M.L. Cohen, Fully Collapsed Carbon Nanotubes, Nature 377 (1995) 135–138.

[5] E. Hernández, C. Goze, P. Bernier, A. Rubio, Elastic Properties of C and BxCyNz Composite Nanotubes, Phys. Rev. Lett. 80 (1998) 54502–4506.

[6] T. Dumitrică, M. Hua, B.I. Yakobson, Symmetry-, Time-, and Temperature-Dependent Strength of Carbon Nanotubes, Proc. Natl. Acad. Sci. USA 103 (2006) 6105–6109.

[7] B.D. Jensen, A. Bandyopadhyay, K.E. Wise, G.M. Odegard, Parametric Study of ReaxFF Simulation Parameters for Molecular Dynamics Modeling of Reactive Carbon Gases, J. Chem. Theory. Comput. 8 (2012) 3003–3008.

[8] C. Zhang, A.C.T. van Duin, J.W. Seo, D. Seveno, Weakening Effect of Nickel Catalyst Particles on the Mechanical Strength of the Carbon Nanotube/Carbon Fiber Junction, Carbon 115 (2017) 589–599.

[9] J.A. Elliott, J.K.W. Sandler, A.H. Windle, R.J. Young, M.S.P. Shaffer, Collapse of Single-Wall Carbon Nanotubes is Diameter Dependent, Phys. Rev. Lett. 92 (2004) 095501.

[10] G. Gao, T. Çağin, W.A.G. III, Energetics, Structure, Mechanical and Vibrational Properties of Single-Walled Carbon Nanotubes, Nanotechnol. 9 (1998) 184–191.

[11] S.J. Marrink, H.J. Risselada, S. Yefimov, D.P. Tieleman, A.H.d. Vries, The MARTINI Force Field: Coarse Grained Model for Biomolecular Simulations, J. Phys. Chem. B 111 (2007) 7812–7824.

[12] J. Tersoff, Empirical Interatomic Potential for Carbon, with Applications to Amorphous Carbon, Phys. Rev. Lett. 61 (1988) 2879–2883.

[13] J.-J. Shang, Q.-S. Yang, X. Liu, New Coarse-Grained Model and Its Implementation in Simulations of Graphene Assemblies, J. Chem. Theory Comput. 13 (2017) 3706–3714.

[14] I. Ostanin, R. Ballarini, T. Dumitrică, Distinct Element Method Modeling of Carbon Nanotube Bundles with Intertube Sliding and Dissipation, J. Appl. Mech. 81 (2014) 061004.

[15] M.J. Buehler, Mesoscale Modeling of Mechanics of Carbon Nanotubes: Self-Assemby, Self-folding, and Fracture, J. Mat. Res. 21 (2006) 2855–2869.

[16] A.N. Volkov, L.V. Zhigilei, Mesoscopic Interaction Potential for Carbon Nanotubes of Arbitrary Length and Orientation, J. Phys. Chem. C 114 (2010) 5513–5531.

[17] I. Ostanin, R. Ballarini, D. Potyondy, T. Dumitrică, A Distinct Element Method for Large Scale Simulations of Carbon Nanotube Assemblies, J. Mech. Phys. Solids 61 (2013) 762–782.

[18] T. Dumitrică, R.D. James, Objective Molecular Dynamics, J. Mech. Phys. Solids 55 (2007) 2206–2236.

[19] I. Nikiforov, E. Dontsova, R.D. James, T. Dumitrică, Tight-Binding Theory of Graphene Bending, Phys. Rev. B 89 (2014) 155437.

[20] J. Al-Ghalith, H. Xu, T. Dumitrică, Collapsed Carbon Nanotubes as Building Blocks for High-Performance Thermal Materials, Phys. Rev. Matt. 1 (2017) 056001.

[21] D. Porezag, T. Frauenheim, T. Köhler, G. Seifert, R. Kaschner, Construction of Tight-Binding-Like Potentials on the Basis of Density-Functional Theory: Application to Carbon, Phy. Rev. B 51 (1995) 12947–12957.

[22] D.-B. Zhang, T. Dumitrică, Effective Strain in Helical Rippled Carbon Nanotubes: A Unifying Concept for Understanding Electromechanical Response, ACS Nano 4 (2010) 6966–6972.

[23] T.F.T. Cerqueira, S. Botti, A. San-Miguel, M. A.L.Marques, Density-Functional Tight-Binding Study of the Collapse of Carbon Nanotubes under Hydrostatic Pressure, Carbon 69 (2013) 355–360.

[24] H. Mehrez, A. Svizhenko, M.P. Anantram, M. Elstner, T. Frauenheim, Analysis of Band-Gap Formation in Squashed Armchair Carbon Nanotubes, Phy. Rev. B 71 (2005) 155421.

[25] D.-B. Zhang, R.D. James, T. Dumitrică, Electromechanical Characterization of Carbon Nanotubes in Torsion via Symmetry-Adapted Tight-Binding Objective Molecular Dynamics, Phys. Rev. B 80 (2009) 115418.

[26] B. Aradi, B. Hourahine, T. Frauenheim, DFTB+, A Sparse Matrix-Based Implementation of the DFTB Method J. Phys. Chem. A 111 (2007) 5678–5684.

[27] R.D. James, Objective Structures, J. Mech. Phys. Solids 54 (2006) 2354–2390.

[28] D.-B. Zhang, M. Hua, T. Dumitrică, Stability of Polycrystalline and Wurtzite Si Nanowires via Symmetry-Adapted Tight-Binding Objective Molecular Dynamics, J. Chem. Phys. 128 (2008) 128.

[29] I. Nikiforov, B. Hourahine, B. Aradi, T. Frauenheim, T. Dumitrică, Ewald Summation on a Helix: A Route to Self-Consistent Charge Density-Functional Based Tight-Binding Objective Molecular Dynamics, J. Chem. Phys. 139 (2013) 094110.

[30] R.P.B. de Santos, E. Perim, P.A.S. Autreto, G. Brunetto, D.S. Galvão, On the Unzipping of Multiwalled Carbon Nanotubes, Nanotechnol. 23 (2012) 465702.

[31] D.-B. Zhang, E. Akatyeva, T. Dumitrică, Bending Ultrathin Graphene at the Margins of Continuum Mechanics, Phys. Rev. Lett. 106 (2011) 255503.

[32] P.A. Cundall and O.D.L. Strack, A Discrete Model for Granular Assemblies, Geotechnique 29 (1979) 47–65.

[33] Y. Wang, H. Xu, G. Drozdov, T. Dumitrică, Mesoscopic Friction and Network Morphology Control the Mechanics and Processing of Carbon Nanotube Yarns. Carbon 139 (2018) 94–104.

[34] PFC3D (Particle Flow Code in 3 Dimensions), Version 5.0. Minneapolis: ICG., 2008.

[35] H. Xu, J. Al-Ghalith, T. Dumitrică, Smooth Sliding and Superlubricity in the Nanofriction of Collapsed Carbon Nanotubes, Carbon 134 (2018) 531–535.

[36] A. Rao, S. Tawfick, M. Bedewy, A.J. Hart. Morphology-dependent load transfer governs the strength and failure mechanism of carbon nanotube yarns. Extreme Mech. Lett. 9 (2016) 55–65.

[37] M. Elstner, The SCC-DFTB Method and Its Application to Biological Systems, Theor. Chem. Acc. 116 (2006) 316–325.

[38] G.M. Grason, Perspective: Geometrically Frustrated Assemblies, J. Chem. Phys. 145 (2016) 110901.